Pore-scale simulations of two-phase flow in granular materials

C. Yuan, B. Chareyre & F. Darve
Laboratoire Sols, Solides, Structures, Grenoble, France
chao.yuan@3sr-grenoble.fr bruno.chareyre@3sr-grenoble.fr
felix.darve@3sr-grenoble.fr

ABSTRACT

A pore-scale model is presented for simulating two-phase flow in granular materials. The solid phase is idealized as dense random packings of polydisperse spheres, generated with the discrete element method (DEM). The pore space is conceptualized as a network of pores connected by throats, which is obtained by using regular triangulation. Theoretical formulas for calculating geometrical properties and entry capillary pressure for given pores are developed by extending the Mayer and Stowe-Princen (MS-P) theory of drainage. Such relationships are employed in the network for defining as local invasion criteria, so that the drainage can be represented by the replacement of W-phase when the threshold value is reached. Different side boundary conditions and the events of W-phase entrapment are considered during the coupling procedures. This pore-scale model is verified by comparing simulation results with experimental data of quasi-static drainage experiments in a synthetic porous medium. The simulated $P^c - S^w$ curve in primary drainage is in agreement with the experimental one.

INTRODUCTION

Understanding transport properties of multiphase flow in porous media is of great importance for many areas of engineering and science, such as oil recovery, agriculture irrigation and environmental restoration. Although most of these problems describe such flow process at the macro-scale, pore-scale modeling provides an important means to improve our understanding of the insight physical processes. In order to simulate large domains, one often represent the porous medium by a pore-network, in which the void space of the medium is represented by a lattice of wide pores connected by narrow throats. Using appropriate physical laws that govern the transport and arrangement of fluids in system, network can then be made to replicate experimental measurements at the microscopic scale (Fatt 1956, Ma et al. 1996, Mayer & Stwoe1965). However, most of those networks are based on regular and structured topology, which can not describe the irregular and unstructured characteristics of porous

medium. Recently, more and more researchers focus their interest on models of realism, in which the topology of networks are based on real porous medium. This approach is pioneered by Bryant and Blunt (Bryant & Blunt 1992, Bryant et al. 1993), who constructed the network based on a measured random packing of equal spheres (Finney pack). With the help of powerful measuring methods and computational techniques, more and more accurate topologically equivalent skeletons are built(Øren et al. 1998, Dong & Blunt 2009).

The method considered in this study is similarly devoted to the pore-scale modeling of the transport process of multiphase flow, but important differences are also noticeable in the geometrical idealization of the pore space and network modeling. These difference are mainly due to the spherical geometry of the solid particles and to the pore space decomposition technique. This study represents a first step in the direction of developing a fully coupled, computationally efficient model combining two-phase flow and deformation in porous media. In particular, we will focus our effort on the faithful approximation of the capillary pressures applied by the fluid-fluid interface on solid grains and of the arrangements of phases displacements, with the aim of incorporate these pressures and arrangements in the discrete element method (DEM) computation.

PORE-SCALE NETWORK

We propose a pore-scale network model to process the decomposition of the porous media. The solid phase is idealized as dense random packings of polydisperse spheres, generated with DEM (Smilauer et al.2010). The decomposition of the pore space is obtained in three dimensions by a using Regular Triangulation method, in which the void of porous media is conceptualized as a network of pores connected by throats. A similar network was introduced recently for the so called the Pore-scale Finite Volume scheme (PFV) for one-phase flow. It is able to reflect in a natural way the deformation of the porous material system. Here it will be discussed briefly; a more detailed description can be found in Chareyre et al. (2012) and Catalano (2012).

Regular Triangulation (or referred as weighted Delaunay triangulation) generalizes classical Delaunay triangulation to weighted points, where weights account for the size of the spheres (Edelsbrunner &Shah 1996). The dual Voronoi graph of regular triangulation is entirely contained in voids between solid spheres. Such network scheme can ideally be assigned to solve the flow path problem within the porous sample. A typical network of Regular Triangulation is shown in Figure 1. Based on this decomposition, a “pore” is bounded by four solid spheres with respective radius $R\{r_1, r_2, r_3, r_4\}$, which are arranged forming a simple tetrahedron packing order. Pore body volume is defined to be the irregular cavity within the tetrahedron (see Figure 2(a)). The shape of pore throat is considered to be the cross section extending within tetrahedral facets, thus the volume of throat is assumed to be 0. Specifically, the geometry of entry pore throat is a critical cross-sectional area quantified by the multiphase contact lines (shown in Figure 2(b)).

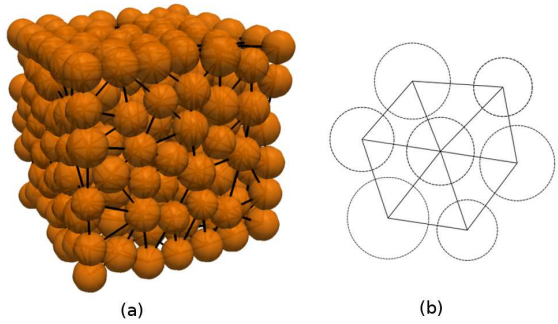

Figure1. **Definition of pore network for packing of spheres, generated by regular triangulation in 3D(a) and 2D(b).**

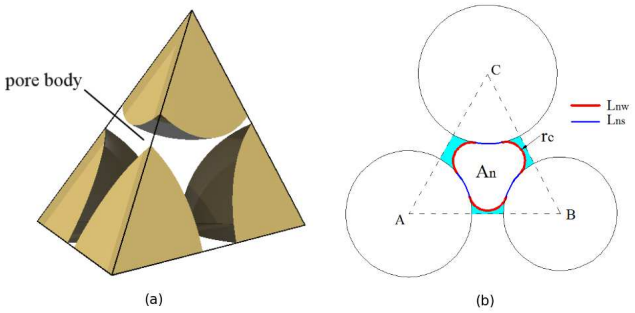

Figure 2. **Pore geometry. (a)A pore defined by tetrahedral element of the finite volume decomposition. (b)Definition of pore throat geometry.** r_c is the curvature of meniscus; L_{nw} is the length of contact line between nonwetting and wetting phases; L_{ns} is the length of contact line between nonwetting and solid phases.

Since each pore is a tetrahedron, it has four neighbors, resulting in a lattice of connectivity four. Although the similar network can be found in other models (Mason 1971, Gladkikh & Bryant 2003), those decomposition techniques are limited by solid particle size, in which the triangulation can only be assigned in packing of equal spheres. In this model, the network definition applies polydisperse sphere packings. The only restriction on this geometrical description is that the center of one sphere should not lie inside another sphere. As such, contact or even moderate overlaps between adjacent spheres are allowed.

DRAINAGE MODEL

Local rules

The phenomena of multiphase flow in porous media can be divided into quasi-static regime and dynamic ones. For two-phase flow, or referred as drainage and imbibition, in the absence of gravity, the conventional immiscible displacement can be described by two dimensionless numbers, the viscosity ratio M and the capillary number C_a,

$$M = \frac{\mu_{inv}}{\mu}, C_a = \frac{\mu v}{\sigma} \tag{1}$$

where μ_{inv} is the viscosity of invading phase, μ is the viscosity of receding phase, v is the receding phase average or macroscopic velocity and σ is the interfacial tension between two

fluid phases (Lenormand et al. 1988, Lenormand 1990). The limit of "quasi-static" flow is defined by C_a closed to 0.

The model we propose is aiming to simulate the primary drainage phenomenon of air-water system, or typically, more generally nonwetting-wetting (NW-W) systems. We hypothesize the drainage process is in a quasi-static regime, in which dynamic effects is in absent and the flow is dominated by capillary forces. Thus, we can neglect the effects of phases viscosity during the process. The porous within a fluid phase is uniform in every connected domain.

The drainage process is controlled by the capillary pressure P^c, i.e., the pressure difference between NW-phase and W-phase. The invasion of one pore is controlled by the associated pore throats. Because the entry capillary pressure of pore body is smaller than that of pore throat, after the invasion of throat, the body is filled by NW-phase spontaneously. In principle, the receding W-phase can be present in the involved domain in the form of disconnected pendular rings left behind. The relationship between the capillary pressure and volume of liquid bridge can be found in our previous research (Scholtes et al. 2009). However, in this model, we assume this volume is negligible. So there is no saturation associated with corner W-phase. Thus the state of a local pore unit is in binary condition, i.e., the pore is either filled with W-phase or with NW-phase.

A relationship between capillary pressure P^c, interfacial tension, σ, and curvature of the NW-W interface, *C*, is given by the Young-Laplace equation,

$$P^c = \sigma C \tag{2}$$

The curvature *C* is fixed by the boundary conditions of NW-phase, W-phase and solid particle surface. For simplicity in the simulation, the solid particle media and pore-network are assumed to be fixed. Commonly in a regular interface, *C* can be acquired from the principal radii of the meniscus (r_1 and r_2) by

$$C = (\frac{1}{r_1} + \frac{1}{r_2}) \tag{3}$$

However, in complex pore geometry, *C* are difficult to define. So a more clearly knowledge of connection among P^c, *C* and pore geometry is required.

Determination of entry capillary pressure

The drainage process is assumed in quasi-static regime, so P^c is applied into porous media to result in from one equilibrium state to another. The NW-phase invasion is locally controlled by entry capillary pressure P_e^c of pore throat. The determination of P_e^c is based on MS-P (Mayer-Stowe-Princen) method, which follows the balance of forces for NW-W interface of pore throat (Princen 1969, Mayer&Stowe 1996).

$$\sum F = F^p + T^\sigma \tag{4}$$

where, F_p is the capillary force acting on pore throat section domain; T^σ is the total tension force along multi-phase contact lines. The same strategy for solving P_e^c can also be found in Ma et al. (1996), Prodanovic & Bryant (2006) and Joekar-Niasar et al. (2010). For completeness, we recall the generic aspect of the MS-P method hereafter.

As described in the previous section, the geometry of pore throat has a mixed cross-sectional shape extending in the facet of tetrahedral pore. Figure 2(b) shows the schematic cross section of a local pore throat formed by solid phase surface and NW-W interface. In local drainage of pore unit, when NW-phase invades pore body, W-phase will remain in the corners of throats along the fictious tube. The longitudinal curvature of the resulting interface inside the tube is zero (Joekar-Niasar et al. 2010). The critical curvature of three menisci extending within throat section, i.e., the curvature of contact lines between NW-phase and W-phase, are equal. Let that radius be denoted by entry capillary radius r_c. Then, following Young-Laplace equation, P_e^c can be written:

$$P_e^c = P^n - P^w = \frac{\sigma^{nw}}{r_c} \tag{5}$$

in which, P^n and P^w are pressure of NW-phase and W-phase; σ^{nw} is NW-W interface tension.

According to the geometry of pore throat we defined in Figure 2(b), the forces acting on interface can be written:

$$F^p = P_e^c A_n \tag{6}$$

$$T^\sigma = L_{nw}\sigma^{nw} + L_{ns}\sigma^{ns} - L_{ns}\sigma^{ws} \tag{7}$$

where, A_n is the area of pore throat section; L_{nw} and L_{ns} are total length of NW-W contact lines and NW-Solid contact lines, respectively. The multiphase interfacial tensions, σ^{ns}, σ^{ws} and σ^{nw} have a relationship with contact angle θ, defined by Young's equation,

$$\sigma^{ns} - \sigma^{ws} = \sigma^{nw}\cos\theta \tag{8}$$

Then Eq.7 will be read,

$$T^\sigma = (L_{nw} + L_{ns}\cos\theta)\sigma^{nw} \tag{9}$$

In a local pore geometry, Eq.6 and Eq.9 can be expressed by the functions of r_c, so the equilibrium state in Eq.4 can be implicitly described by r_c:

$$\sum F(r_c) = F^p(r_c) + T^\sigma(r_c) = 0 \tag{10}$$

Function of $\sum F(r_c)$ is monotonic; the value boundary of r_c can be obtained by following the geometry of pore throat. Therefore, r_c can be solved by numerical technique. Finally, P_e^c can be determined by Eq.5.

Drainage and entrapment of W-phase

Each tetrahedral pore has four neighboring pores, thus the coordination number in 3-D is four. In order to explain the invasion logic of our model, herein we project the system of 3-D network to a 2-D lattice mapping (see Figure 3). Pore bodies and throats are represented by squares and line bondings respectively. Different flags are assigned to the pores for tracking the flow path, which can dynamically record the pore states and the connectivity of different regions with the reservoirs. A search algorithm is employed for updating those states during invasion.

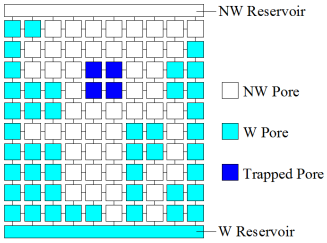

Figure 3. **Demonstration of NW-phase invasion and W-phase trapping in network (in 2D mapping for clarify).**

Initially, the porous media is saturated, and the top and bottom boundaries are connected to NW and W reservoirs, respectively. The effect of gravity is ignored. Drainage starts by increasing the capillary pressure P^c, in which we increase the local pressure of NW reservoir P^n and keep local pressure of W reservoir P^w constant. A search is executed on the pore throats which are connecting with NW reservoir, to locate the easiest entrance for invasion. The first phase displacement, or referred as Haines jump, happens when local P^c surpasses the minimum threshold, e.g. the local entry capillary pressure $P_e^c(i)$ of pore unit *i*. After pore *i* being drained, a second judgment is performed on the neighbor pore of *i*, e.g. pore *j*. If P^c is also larger than $P_e^c(j)$, pore *j* will be drained as well. Such NW-phase percolation will be performed until no more pores can be drained. Then a new equilibrium is achieved, and the state flags are updated for next step of drainage. So the Haines jump events maybe not only displace the W-phase pore-by-pore, but could also involve pore clusters. Such discontinuous changes of the W-phase content can also be verified by experimental tests (Prodanovic & Bryant 2006).

As the NW-phase is invading, the W-phase maybe forms clusters which are disconnected with the W reservoir. We propose the model being in a quasi-static regime, so the entrapped W-phase will remain stationary even if local P^n is growing. The evacuation of pore unit is hypothesized to be binary; therefore, the trapped W-phase will be the only factor that affects residual saturation. In order to identify these entrapment events, a dynamic search rule is employed during each step of drainage by assigning a Trapped Pore flag (as seen in Figure 3).

In the model, W-phase is assumed to be incompressible, so the geometry of trapped cluster will remain unchanged ever since it forms. According to Equ.(2), P^c will also remain the same because of unchanging of NW-W interfacial curvature. Therefore, P^w of trapped W-phase will grow along with the increasing of local P^n. Since the disconnections of different regions may happen on time sequential, P^w of trapped clusters will show diversity.

Boundary conditions

In our model, the evolution of NW-phase invasion is considered to be a finite-size problem, thus we only focus our interest on the case of non-periodic boundary condition (NPBC). Although the Regular Triangulation operation in PFV scheme is able to achieve the network with periodic boundary condition (PBC), the related study will be deferred to our further publication. In NPBC scenario of PFV model, the boundaries are in the form of spheres with near-infinity radii for obtaining the triangulation procedure. Thus, there are no new special cases of plane geometry that are introduced in the model, and all equations and algorithms presented in previous sections can be utilized for boundaries.

We assign top and bottom boundary layers of pore units connecting with NW and W reservoirs, respectively, in which case the state flags of those pores will not change during invasion. Correspondingly, the calculation of saturation will not involve the volume of these boundary pores.

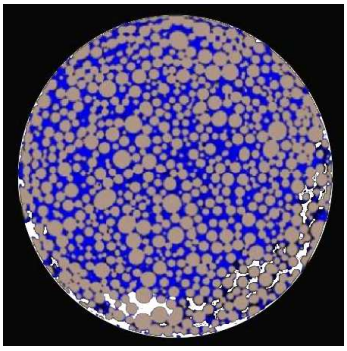

Figure 4. **Experimental scan through the cross-section of glass beads column by G. Khaddour. Brown (gray) circle regions are glass beads, blue (dark) regions are water, and white regions are air. See color version of this figure in the HTML.**

Another consideration in NPBC is the connectivity of side boundary pores, i.e., the sides are assumed to be open or closed. In the usual case, the porous medium is located in a regular container in the experimental test, so the side pore throats are open, or referred as a permeable boundary condition. The pores contacting with side boundary of container can be drained much easier than inside ones, in which case early Haines jumps can be observed in side domain, because the side boundary pore, which is composed by solid particles and smooth container wall, has relatively larger pore throat and the P_e^c trend to be smaller. This priority of invasion event has been verified by experiment test (Khaddour 2012). As shown in Figure 4, the NW-phase firstly penetrates into the void between glass beads and the container, and then invades the pores composed by glass beads. It is worthwhile to note that this percolation sequence is only adapted to spherical granular material test. If the drainage experiment is operated with irregular shape porous media, the composition of side pores will be different, and the priority of invasion needs further discussion. In some special cases, the side pore throats are closed, corresponding to an impermeable boundary condition, which means there is no fluid exchange between the side voids and the porous media. The different side boundary conditions can significantly influence the drainage patterns and residual saturation (Chandler et al. 1982). Therefore, to accommodate different scenarios, we perform both of situations, named open-side drainage and close-side drainage. In open-side drainage, NW-phase can go through the space between porous medium and side boundary of container (corresponding to a permeable boundary condition); while in close-side drainage, the Haines jump can only happen inside the porous medium (corresponding to an impermeable boundary condition). The calculations of saturation are adapted to different scenarios as well.

Implementation

The network by using Regular Triangulation, which is based on PFV scheme (Chareyre et al. 2012), has been implemented in C++. The C++ library CGAL (Boissonnat et al. 2002) is used for the regular triangulation procedure. Geometry for determination of entry capillary pressure and local drainage rules are also implemented in this model with C++. This pore-scale network is freely available as an optional package of the open-source software Yade (Smilauer et al. 2012).

The CGAL library insures exact predicates and constructions of network. The only nontrivial operation is the computation of entry phase curvature needed to define the NW-W phase contact lines and pore throat areas to determine acting forces in Equ.(10). As mentioned in previous section, open-side and close-side drainage modes are assigned according to optional side boundary conditions.

COMPARISON WITH EXPERIMENT

Numerical setup

In this section, we verify the pore-network model by comparing the simulation results with experimental data of quasi-static drainage experiment in a synthetic porous medium (Culligan et al. 2004). The medium consisted of packed glass beads, which are contained in a column of 70 mm in length and 7 mm in diameter. The particle size distribution (PSD) of glass beads is given in Table.(1), with a porosity of 0.34. Drainage is carried out by pumping water out of the porous medium with a certain flow rate to maintain the system to equilibrate. A 5 mm section of the column is imaged by using X-ray micro-tomography to obtain capillary pressure-saturation ($P^c - S^w$) relationship.

Weight(%)	Diameter(mm)
30	1.0-1.4
35	0.850
35	0.600

Table 1. **Particle size distribution of porous medium**

In the simulation, it's unachievable to assign the pore-network (Regular Triangulation) in geometry of circular column, so we compromise by implementing model in cuboid packings. Following the experimental scene, the simulation packing is connected to the NW reservoir on the top, and to the W reservoir at the bottom. However, the scanned domain emulated by our model is only a small part of a large column, in which case the assumption of connection between pore units of top layer and NW reservoir boundary is still ambiguous. Because for low capillary number, flow in porous medium is dominated by capillary forces, leading to capillary fingerings regime in the column. Thus in the scanned domain, the scope of connectivity between pores of top layer and NW reservoir is unclear. We can assume only some big pores connecting with invading phase reservoir or all of them involving this connection. Both of the hypotheses are reasonable if we only plan to simulate part of the volume or sections of experimental tests, but the results will be significantly different. The similar numerical comparison and conclusions can also be found in Joekar-Niasar et al. (2010). To extricate this predicament, we implement the simulation in a slightly larger size of container. The scanned region of data analyzed in experiment are 4.522 mm, 5.117 mm and 4.964 mm in the x, y and z direction, and the average grain size for the distribution of beads is 0.8675 mm. We assign the simulation in a cuboid packing with 7 mm in side length, in which 800 spheres are distributed randomly, assuming the pores of top boundaries are all connected with invading phase reservoir. But the quantitative study of $P^c - S^w$ relationship is only manipulated on the cuboid sub-domain with 5 mm in side length. The connectivity between sub-domain and reservoir is locally determined by the pore geometry. According to the setup of experiment, we suppose the NW-phase can invade from side boundary, thus open-side drainage mode is assigned.

In the research, we couldn't manage to achieve the original positioning data of glass beads in benchmark experiment. But the porous medium with target PSD and porosity can be easily emulated by using our DEM software by the growth of spheres after randomly positioning, using the radius expansion-friction decrease (REFD) growth algorithm of (Chareyre et al. 2002). So we compromise to simulate a series of repeated test on different randomly positioning packings with the consistent PSD and porosity of the experiment. In order to compare conveniently with all simulation cases, the simulation results and experiment data are both normalized to be dimensionless quantities. We represent the capillary pressure P^c by,

$$P^* = \frac{P^c \overline{D}}{\sigma^{nw}} \tag{10}$$

in which, $\overline{D}$=0.8675 mm is the average size for PSD, σ^{nw} = 7.28 × 10−2N⁄m is the W-phase (water) surface tension in contact with NW-phase (air) in 20 ^{o}C. We also assume the material of solid particles is perfectly wetting, so the contact angle θ in simulation is 0.

Comparison results and discussion

Using the technique described above, we compute the primary drainage process of 100 randomly positioning packings with the same PSD and porosity. Figure 5 presents the results of these simulations, in which we gather all scattered (S^w, P^*) points of each simulation in one image. As shown in Figure 5, although all packings share the same macro-mechanics parameters, the $P^c - S^w$ curves still have a distinct variety because of micro setup, i.e., sphere positioning. Especially, the residual saturation has a great difference. This erratic dispersion can be reduced by enlarging the simulation scales. The (P^c, S^w) variables associating with the representative elementary volume will be deferred to our further publication. We compare the average results from 100 repeating simulations with the experimental data. It shows satisfactory agreement between predicated capillary curve and obtained experimentally by Culligan et al. (2012). The unremarkable difference is mainly caused by the different specimen shapes, i.e., the simulation using cuboid column packing and experiment using circular column one.

We capture one test from the series of simulation and cut a slice to observe the characteristics of invasion as shown in Figure .6. By increasing P^c, the invasion starts from the pores with larger throat, in which the entry capillary pressure is smaller (see slice (a)). As described in previous section, the P_e^c of side pore throats usually relative smaller than that of inside pore throats, so the NW-phase invade from side pores first (as shown in Figure 6(a) and (b)). By comparing slices (b) and (c), we can find out that at certain circumstances even a slight changing in P^c can cause a notable NW-W interface movement. So such event, i.e., Haines jump, can involve a cluster of pores, causing a obvious discontinuous decrease of W-phase content. In slice (d) showing the finish of test, even under a large P^c, there is no changing in saturation, which means such W-phase is entrapped by NW-phase.

In the model, it's assumed that the W-phase transport by film flow or evaporation is negligible, so even if we keep increasing local P^c, the trapped W-phase will stay stationary. As explained in previous section, the trapping events happen in sequentiality, and the W-phase is supposed to be incompressible, thus the inner wetting pressure P^w of different trapped cluster show a diversity as shown in Figure 7. From the pressure distribution, we can

determine the order of occurrence of disconnections, in which the larger trapped P^w means the earlier happening of entrapment.

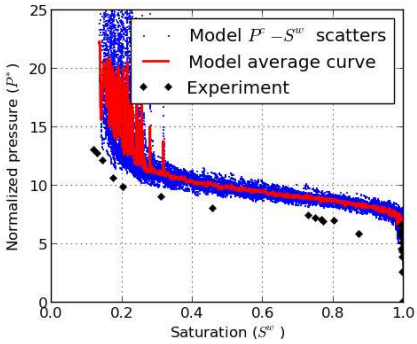

Figure 5. **Comparison between simulation and experiment for primary drainage $P^c - S^w$ curves. The No. of observations of simulation is 100.**

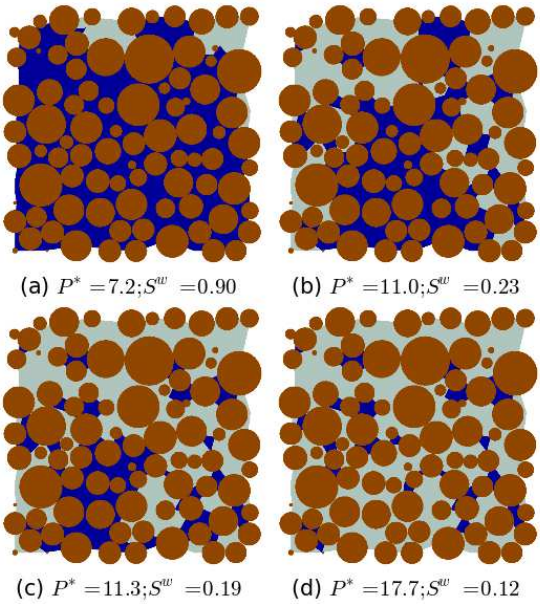

Figure 6. **The process of drainage (800 particles), NW-phase invade from top. Brown (gray) is solid phase, blue (black) is W-phase, and light cyan (white) is NW-phase, see color version of this figure in the HTML.**

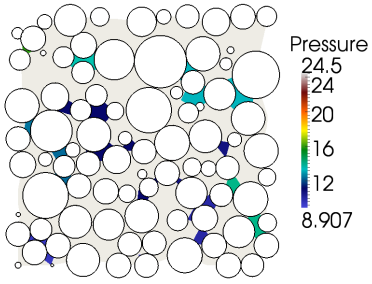

Figure 7. **Distribution of capillary pressure. White circle is solid, light region is NW-phase pressure P^n, dark regions are W-phase pressures P^w, see color version of this figure in the HTML.**

CONCLUSION

A pore-scale network model of quasi-static two-phase flow in dense sphere packings has been proposed. The model can satisfactorily replicate the phenomenon of primary drainage in synthetic porous medium. The pore space is efficiently represented by means of a Regular Triangulation and the entry pore throat geometry is mathematically determined by the equilibrium of the pore system. The key methods of this model are the calculation of the entry capillary pressure applied by the fluids and the prediction of the displacements of phases. Expressions of the local capillary force and tension force induced on the NW-W interface of pore throat have been derived, which are based on Young-Laplace equation and local pore geometry. The definition of entry capillary pressure is based on MS-P (Mayer-Stowe-Princen) method, which follows the balance of forces for NW-W interface in quasi-static regime. The drainage process is represented by the invasion of NW-phase when the threshold value is reached.

One key feature of the model is its capability to entrap the receding W-phase, indicating the residual saturation. A dynamic search algorithm is applied to identify whether local disconnection causes large clusters of wetting pores to get disconnected with wetting phase reservoir. Another key feature is its optional side boundary condition. To accommodate different experimental situations, the pore throats of side boundary can be considered open or closed, corresponding to the permeable or impermeable boundary conditions. For validation purpose, the model has been used for simulating primary drainage experiments carried out in a glass bead packing. The simulated $P^c - S^w$ curve is in agreement with experiment one, which means the capability of the pore-scale network model for simulating a real porous medium can be verified.

ACKNOWLEDGEMENTS

The authors want to acknowledge G. Khaddour and S. Salager for discussions and sharing us the experimental images, and G.Viggiani for suggesting this cooperation work.

REFERENCES

Bear, J. 1972. Dynamics of fluids in porous media., American Elsevier, New York.

Boissonnat, J., Devillers, O., Pion, S., Teillaud, M. & Yvinec, M. 2002. Triangulations in cgal, *Computational Geometry: Theory and Applications* 22: 5–19.

Bryant, S. & Blunt, M. 1992. Prediction of relative permeability in simple porous media, *Phys. Rev. A* 46 : 2004–2011.

Bryant, S., King, P. & Mellor, D. 1993. Network model evaluation of permeability and spatial correlation in a real random sphere packing, *Transport in Porous Media* 11 (1): 53–70.

Catalano, E. 2012. A pore-scale coupled hydromechanical model for biphasic granular media, *Ph.D. thesis*, Grenoble INP.

Chandler, R., Koplik, J., Lerman, K. & Willemsen, JF. 1982. Capillary displacement and percolation in porous media, *Journal of Fluid Mechanics* 119: 249–267.

Chareyre, B., Briancon, L.& Villard, P. 2002. Theoretical versus experimental modelling of the anchorage capacity of geotextiles in trenches., *Geosynthetics International* 9 (2): 97–123.

Chareyre, B., Cortis A., Catalano E., & Barthelemy E. 2012. Pore-scale modeling of viscous flow and induced forces in dense sphere packings, *Transp. Porous Med.* 92: 473–493.

Cundall, P. & Strack, O. 1979. A discrete numerical model for granular assemblies, *Geotechnique* (29): 47–65.

Culligan, K., Wildenschild, D., Christensen, B., Gray, W., Rivers, M., & Tompson, A. 2004. Interfacial area measurements for unsaturated flow through a porous medium, *Water Resour. Res.* 40 (12).

Dong, H. & Blunt, M. 2009. Pore-network extraction from micro-computerized tomography images, *Phys. Rev. E* 80: 036307.

Dullien, F. 1992. Porous Media: Fluid Transport and Pore Structure, Academic, San Diego, Calif.

Edelsbrunner, H. & Shah, NR. 1996. Incremental topological flipping works for regular triangulations, *Algorithmica* 15 (6): 223–241.

Fatt, I. 1956. The network model of porous media, *Trans AIME* 207: 144–181.

Gladkikh, M. & Bryant, S. 2003. Prediction of interfacial areas during imbibition in simple porous media, *Advances in Water Resources* 26 (6): 609 –622.

Hilpert, M. & Miller, C. 2001. Pore-morphology-based simulation of drainage in totally wetting porous media, *Advances in Water Resources*. 24 (34): 243 – 255.

Joekar-Niasar, V., Prodanovic, M., Wildenschild, D. & Hassanizadeh, S. 2010. Network model investigation of interfacial area, capillary pressure and saturation relationships in granular porous media, *Water Resour. Res.* 46.

Khaddour, G. 2012. Microscopic mechanisms related to water retention in sand, *Master's thesis*, Universite Joseph Fourier Grenoble.

Lenormand, R. 1990. Liquids in porous media, *Journal of Physics: Condensed Matter* 2 (S): SA79.

Lenormand, R., Touboul, E., & Zarcone, C. 1998. Numerical models and experiments on immiscible displacements in porous media, *Journal of Fluid Mechanics* 189: 165–187.

Ma, S., Mason, G. & Morrow, N. 1996. Effect of contact angle on drainage and imbibition in regular polygonal tubes, *Colloids and Surfaces A: Physicochemical and Engineering Aspects* 117 (3): 273 – 291.

Mason, G. 1971. A model of the pore space in a random packing of equal spheres, *Journal of Colloid and Interface Science* 35 (2): 279 – 287.

Mayer, R. & Stowe, R. 1965. Mercury porosimetrybreakthrough pressure for penetration between packed spheres, *Journal of Colloid Science* 20 (8): 893 – 911.

Øren, P., Bakke, S., & Arntzen, O. 1998 Extending predictive capabilities to network models, *SPE Journal* 3 (4): 324–336.

Princen, H. 1969. Capillary phenomena in assemblies of parallel cylinders: Ii. capillary rise in systems with more than two cylinders, *Journal of Colloid and Interface Science* 30 (3): 359 – 371.

Prodanovic, M. & Bryant, S. 2006. A level set method for determining critical curvatures for drainage and imbibition, *Journal of Colloid and Interface Science* 304 (2): 442 – 458.

Scholtes, L., Hicher, P., Nicot, F., Chareyre, B. & Darve, F. 2009. On the capillary stress tensor in wet granular materials, *Int. J. Numer. Anal. Meth. Geomech.* 33 (10): 1289–1313.

Stark, CP. 1991. An invasion percolation model of drainage network evolution, *Nature* 352 (6334): 423–425.

Smilauer, V., Catalano, E., Chareyre, B., Dorofeenko, S., Duriez, J., Gladky, A., Kozicki, J., Modenese, C., Scholtes, L., Sibille, L., Stransky, J. & Thoeni, K.. 2010. Yade Reference Documentation, *Yade Documentation*. http://yade-dem.org/doc/.